

Generation and application of bursting dynamic behaviour in memristor neurons

Yeheng Bo,¹ Shuai Li,² Peng Zhang,¹ Juan Song,³ and Xinjun Liu^{1, a)}

¹*Tianjin Key Laboratory of Low Dimensional Materials Physics and Preparation Technology, Faculty of Science, Tianjin University, Tianjin 300354, People's Republic of China*

²*Unité Mixte de Physique, CNRS, Thales, Université Paris-Sud, Université Paris-Saclay, Palaiseau, France*

³*Department of Emergency Medicine, Putuo District Central Hospital, Shanghai University of Traditional Chinese Medicine, Shanghai 200062, People's Republic of China*

The memristor neurons built with two memristors can be used to mimics many dynamical behaviours of a biological neuron. Firstly, the dynamic operating conditions of memristor neurons and their transformation boundaries between the spiking and the bursting are comprehensively investigated. Then, the underlying mechanism of bursting is analysed and the controllability of the number of spikes in each burst period is demonstrated under proper input voltage and input resistor. Final, numbers of spikes per period is recognized as neuron information carries and shown to enable pattern recognition and information transmitting. These results show a promising approach for the efficient use of neuristor in the construction of neural networks.

Keywords: Memristor; Neuron; Dynamic behaviour

^{a)} Electronic mail: xinjun.liu@tju.edu.cn

I. Introduction

Neuromorphic computing based on artificial neural network has received extensive attention due to its low energy consumption. The higher power consumption in conventional CMOS hardware limit the implementation of data driven artificial intelligence based on the von Neumann framework[1]. Although the energy consumed in the calculation can be reduced by updating the algorithm, the energy-efficiency problem cannot be improved significantly. Replacing a portion of a CMOS components with other functional materials can implement an artificial neural network circuit using fewer components and lower power consumption than conventional CMOS[2, 3].

A two-terminal metal–insulator–metal device exhibits current-controlled negative differential resistance (CC-NDR), also known as active memristor[4, 5]. Memristor is one of the hardware candidates for neuromorphic computing because of its low power consumption, plasticity and compatibility with conventional CMOS[4, 6, 7]. Artificial neuron, one of the most important elements of artificial neural networks, require many components to be implemented on CMOS[8]. Pickett et al.[9, 10] used two Mott memristors to construct a neuristor and realized the four basic neuronal functions as: all-or-nothing spiking of an action potential, a bifurcation threshold to a continuous spiking regime, signal gain and a refractory period. The realization of memristor neurons greatly reduces the power consumption and the number of components of artificial neurons. Yi et al.[11] achieved 23 types of biological neuronal behaviors in memristor neurons, indicating that they possess most of the known biological neuronal dynamics. Using only two memristors and several R , C elements can achieve rich neuron dynamics that can be achieved with thousands of logic gates[12]. The power of memristor neurons is greatly reduced, and the computational complexity will increase when more dynamic behaviour is used in the computing. However, there is still a lack of research on the state dynamics and operational window of the neuronal behaviours caused by input signals. This results in many memristor neuron dynamics that cannot be effectively utilized. The understanding of neurons is beneficial for construction of artificial neural networks.

In this work, we investigated the transformation conditions and operating boundary of memristor neurons. The effect of input resistance and capacitance on the bursting

behavior of memristor neuron was studied. The memristor neuron was incorporated in a 9×1 array to construct the preceptor to prove its potential for neuromorphic computing. Steady information spreading between neurons is also demonstrated.

II. Circuit and model for memristor neuron

Fig. 1a shows a biological neuron that generates an action potential in the direction of an output synapse after receiving sufficient stimulus from dendrites. Fig. 1b shows the circuit diagram of memristor neuron. The ion (K^+ or Na^+) channel consists of a memristor and an opposite voltage source. Capacitors C_1 and C_2 in parallel with the ion channel are membrane capacitors. The resistor R_2 couples the two channels together with the input resistor to form a memristor neuron. Memristor neuron dynamics will change due to different input signals by adjusting the input resistance R_{in} and input voltage V_{in} . The dynamic behavior of the output voltage V_{out} of memristors neuron is important for the construction of neural networks.

Lim et al.[13] approximated the resistance of the memristor to a hard switching between two preset resistance values of R_{on} and R_{off} , and calculated the boundaries A and B of the memristor neuron that can generate spike when one of the memristors X_1 or X_2 is in the critical state of switching, as shown in Fig. 1c and 1d. However, memristor is a non-linear resistor, and the memristor resistance at the critical state is different from R_{on} and R_{off} , which results in inaccurate theoretical boundaries.

A resistor R_{th} at the threshold voltage and a resistor R_h at the hold voltage are introduced, as shown in Fig. 1e. Fig. 1f shows the operational window $R_{in}-V_{in}$ of the simulated (the parameters used for simulation and calculation are shown in Table S1 and S2 in the supplementary material 1). The operational window diagram is divided into three main areas: failure to fire (white), periodic spike (blue), bursting spike (green). The theoretical boundaries after the introduction of R_h and R_{th} are optimized from A (or B) to A' (or B'), which are consistent with the simulated window diagram (see Equations S3, S4, S7 and S8 in the supplementary material 2).

Interestingly, a new boundary C' for the two dynamic transformations between continuous spike and bursting spike is theoretically introduced considering that X_1 and X_2 are simultaneously in the critical state of transition (see Equations S5 and S6 in the supplementary material 2), and the calculated boundary is consistent with the simulated boundary. According to the calculation formula of the three boundary lines, we can design the desired window size of the spike and bursting spike.

III. Controllable bursting under the DC input voltage

Generally, every bursting spike possesses two oscillations components: a fast spiking oscillation within a single burst (inter-spike oscillation), and one modulated by a slow oscillation between the bursts (inter-burst oscillation)[14]. In memristor neuron, V_K represents fast spiking oscillation and V_{Na} represents slow oscillation. Fig. 2a-e are the waveform of V_{Na} and V_K when the capacitance is $C_1=2$ nF, 2 nF, 2 nF, 3.5 nF, 5 nF, $C_2=0.2$ nF, 0.3 nF, 0.5 nF, 0.5 nF, 0.5 nF, respectively. Eqs. (1) and Eqs. (2) show the charge and discharge speed of V_{Na} and V_K :

$$\frac{dV_{Na}}{dt} = \frac{1}{C_1} \left(\frac{V_{in}-V_{Na}}{R_{in}} + \frac{V_K-V_{Na}}{R_2} - \frac{V_{Na}-V_1}{R_{X1}} \right) \quad (1)$$

and

$$\frac{dV_K}{dt} = \frac{1}{C_2} \left(\frac{V_{Na}-V_K}{R_2} - \frac{V_K-V_2}{R_{X2}} \right) \quad (2)$$

respectively. The increase of C_2 will cause the charge and discharge speed of V_K to decrease, which will make the oscillation period of V_K larger, as shown in Fig. 2a-c. The increase of C_1 will cause the charge and discharge speed of V_{Na} to decrease, which will make the oscillation period of V_{Na} larger, as shown in Fig. 2c-e. The mismatch between the charge and discharge speed of V_{Na} and V_K produces bursting spikes. Fig. 2f shows the relationship between C_1/C_2 and the number of spikes in each burst period. The rise in C_1/C_2 will lead to an increase in the number of spikes in each burst period. The charge and discharge speed of V_{Na} and V_K can be regulated not only by C_1 and C_2 , but it can also be regulated by other parameters. So V_{in} , V_1 , V_2 , R_{in} , R_2 , R_{X1} and R_{X2} in equations (1) and (2) can also be used to control the number of pulses.

To demonstrate the bursting spike behaviours in detail, the R_{in} - V_{in} phase diagram was plotted with $C_1=5$ nF and $C_2=0.5$ nF, as shown in Fig. 3a. The phase diagram is divided into three main areas: failure to fire (white), spike (blue), bursting spike (other colors). In bursting spike area, the number of 3 spikes (olive) and 4 spikes (pink) in each burst period were observed with different condition of V_{in} and R_{in} .

When the C_1 increased to 10 nF with fixed C_2 of 0.5 nF, 5 spikes (green), 6 spikes (orange), 7 spikes (cyan), 8 spikes (purple) and 9 spikes (red) per period were

observed in bursting spike area as shown in Fig. 3b. The number of spikes per period can be regulated by adjusting input voltage and input resistance. This means that the number of spikes in each burst period can be regulated by the input signal. When the C_1 increased from 5 nF to 10 nF with fixed C_2 of 0.5 nF, the range of the number of spikes in each burst period increases from 3-4 to 5-9.

The input signal amplitude is fixed at 400 mV and the input resistance varies within the range in which the bursting spike is generated, and the effect of different C_1 on the maximum range of the number of spikes in each burst period, as shown in Fig. 3c. Capacitor C_1 changing from 5 nF to 25 nF results in the range of the number of spikes in each burst period increases from 3-4 (2) to 14-22 (9). Larger the range of spikes can carry more information, which is very important in pattern recognition and neuromorphic computing[15, 16].

IV. Preceptor design for pattern recognition

The main function of the preceptor is to transform the input signal into an output signal through an activation function. In order to facilitate the construction of the array, we use a simple symbol to represent the memristor neuron circuit, as shown in Fig. 4a. We used resistors as input synapses and memristor neurons as neurons to build a 9×1 array, as shown in Fig. 4b. Except for $C_1 = 25$ nF, the rest of the memristor neurons used in the simulation are derived from Table S1. To prove that bursting behaviour can be used for pattern recognition, synaptic resistances are programmed with different weights. Three letter patterns, ‘n’, ‘z’ and ‘v’ were used as inputs as shown in Fig. 4c. Nine squares correspond to the inputs of each synapse. A gray square means a 0.6 V input and a white square means a 0.1 V input. The number of spikes in each burst period corresponding to the three different modes ‘n’, ‘z’, and ‘v’ is 16, 17, 18. This shows that the bursting behavior of memristor neurons has the potential for pattern recognition. The number of spikes in each burst period of bursting are candidates for encoding which is different from the traditional oscillation phase and frequency[17, 18].

V. Information transition by bursting spike

Biological neurons can receive the input of the neurons in the previous layer as the output, and the biological neurons can also be used as the input of the neurons in the next layer. We connected three memristor neurons in series with two resistors to

prove that the bursting behavior of memristor neurons can be transmitted from the upper neuron to the next neuron, as shown in Fig. 5a. When $C_1 = 10$ nF and $C_2 = 1$ nF in neuron N_1 , $C_1 = 3$ nF and $C_2 = 0.3$ nF in neuron N_2 , $C_1 = 1$ nF and $C_2 = 0.08$ nF in neuron N_3 , $R_m = 10$ k Ω , $R_n = 10$ k Ω and $R_q = 15$ k Ω , bursting behavior can stably propagate from the neuron in the previous layer to the neuron in the next layer, as shown in Fig. 5b. Neuron N_1 generates bursting signals at the input of a DC voltage source. Subsequently, a bursting signal with the number of 5 spikes in each burst period generated by neuron N_1 will excite the next neuron N_2 , and neuron N_2 will generate the same number of spikes in each burst period after a short delay after N_1 excitation. Compared with the bursting of neuron N_1 , the number of spikes in each burst period of neuron N_2 is the same, but inter-spike period of neuron N_2 is shorter. Similarly, neuron N_3 can receive the bursting signal generated by neuron N_2 , thereby generating a bursting signal of the same number of spikes in each burst period but with a shorter inter-spike period. When $C_1 = 8$ nF and $C_2 = 4$ nF in neuron N_1 , $C_1 = 3.5$ nF and $C_2 = 2$ nF in neuron N_2 , $C_1 = 2$ nF and $C_2 = 1$ nF in neuron N_3 , $R_m = 10$ k Ω , $R_n = 10$ k Ω and $R_q = 15$ k Ω , a single spike can also spread between neurons, as shown in Fig. 5c. This shows that the bursting signal can keep the number of spikes in each burst period transmitted from the memristor neuron in the previous layer to the memristor neuron in the next layer.

VI. Conclusion

In conclusion, we investigated the dynamic richness and the transition conditions between different dynamic behaviours of neuristor. The memristor model is used to calculate the three theoretical boundaries of the memristor neuron dynamics transformation. The three boundaries are consistent with the simulation. We explored the impact of C_1 and C_2 on bursting. The rise in C_1/C_2 will lead to an increase in the number of spikes in each burst period. When C_1 becomes larger, the range of the number of spikes per period increases, and the bursting can carry more information. Simple pattern recognition was achieved using memristor neurons, and bursting was demonstrated to have the potential for neuromorphic computing. Bursting has been shown to stably propagate from the upper memristor neuron to the next memristor neuron. This enriches the dynamics of neuromorphic computing.

Acknowledgements

This work was supported by the National Natural Science Foundation of China (No. 11674241 and No. 11774253) and Natural Science Foundation of Tianjin City (No. 18JCYBJC18000).

REFERENCES

- [1] Frank D J, Dennard R H, Nowak E, Solomon P M, Taur Y and Wong H-S P 2001 Device scaling limits of Si MOSFETs and their application dependencies *Proceedings of the IEEE* **89** 259-88
- [2] Jeong D S, Kim I, Ziegler M and Kohlstedt H 2013 Towards artificial neurons and synapses: a materials point of view *RSC Advances* **3** 3169-83
- [3] Zhang X, Wang W, Liu Q, Zhao X, Wei J, Cao R, Yao Z, Zhu X, Zhang F and Lv H 2017 An artificial neuron based on a threshold switching memristor *IEEE Electron Device Letters* **39** 308-11
- [4] Pickett M D and Williams R S 2012 Sub-100 fJ and sub-nanosecond thermally driven threshold switching in niobium oxide crosspoint nanodevices *Nanotechnology* **23** 215202
- [5] Shukla N, Joshi T, Dasgupta S, Borisov P, Lederman D and Datta S 2014 Electrically induced insulator to metal transition in epitaxial SmNiO₃ thin films *Applied Physics Letters* **105** 012108
- [6] Xia Q, Robinett W, Cumbie M W, Banerjee N, Cardinali T J, Yang J J, Wu W, Li X, Tong W M and Strukov D B 2009 Memristor– CMOS hybrid integrated circuits for reconfigurable logic *Nano letters* **9** 3640-5
- [7] Yi W 2019 Active Memristor Neurons for Neuromorphic Computing. HRL Laboratories, LLC. Malibu, United States)
- [8] Indiveri G, Linares-Barranco B, Hamilton T J, Van Schaik A, Etienne-Cummings R, Delbruck T, Liu S-C, Dudek P, Häfliger P and Renaud S 2011 Neuromorphic silicon neuron circuits *Frontiers in neuroscience* **5** 73
- [9] Pickett M D, Medeiros-Ribeiro G and Williams R S 2013 A scalable neuristor built with Mott memristors *Nature materials* **12** 114
- [10] Pickett M D and Williams R S 2013 Phase transitions enable computational universality in neuristor-based cellular automata *Nanotechnology* **24** 384002
- [11] Yi W, Tsang K K, Lam S K, Bai X, Crowell J A and Flores E A 2018 Biological plausibility and stochasticity in scalable VO₂ active memristor neurons *Nature communications* **9** 4661
- [12] Cassidy A S, Merolla P, Arthur J V, Esser S K, Jackson B, Alvarez-Icaza R, Datta P, Sawada J, Wong T M and Feldman V 2013 Cognitive computing building block: A versatile and efficient digital neuron model for neurosynaptic cores: IEEE) p 1-10
- [13] Lim H, Kornijcuk V, Seok J Y, Kim S K, Kim I, Hwang C S and Jeong D S 2015 Reliability of neuronal information conveyed by unreliable neuristor-based leaky integrate-and-fire neurons: a model study *Scientific reports* **5** 9776
- [14] Izhikevich E M 2007 *Dynamical systems in neuroscience*: MIT press)
- [15] Woo J, Wang P and Yu S 2019 Integrated Crossbar Array With Resistive Synapses and Oscillation Neurons *IEEE Electron Device Letters* **40** 1313-6

- [16] Lee D, Kwak M, Moon K, Choi W, Park J, Yoo J, Song J, Lim S, Sung C and Banerjee W 2019 Various Threshold Switching Devices for Integrate and Fire Neuron Applications *Advanced Electronic Materials* 1800866
- [17] Corti E, Gotsmann B, Moselund K, Stolichnov I, Ionescu A and Karg S 2018 Resistive Coupled VO₂ Oscillators for Image Recognition: IEEE) p 1-7
- [18] He W, Huang K, Ning N, Ramanathan K, Li G, Jiang Y, Sze J, Shi L, Zhao R and Pei J 2014 Enabling an integrated rate-temporal learning scheme on memristor *Scientific reports* **4** 4755

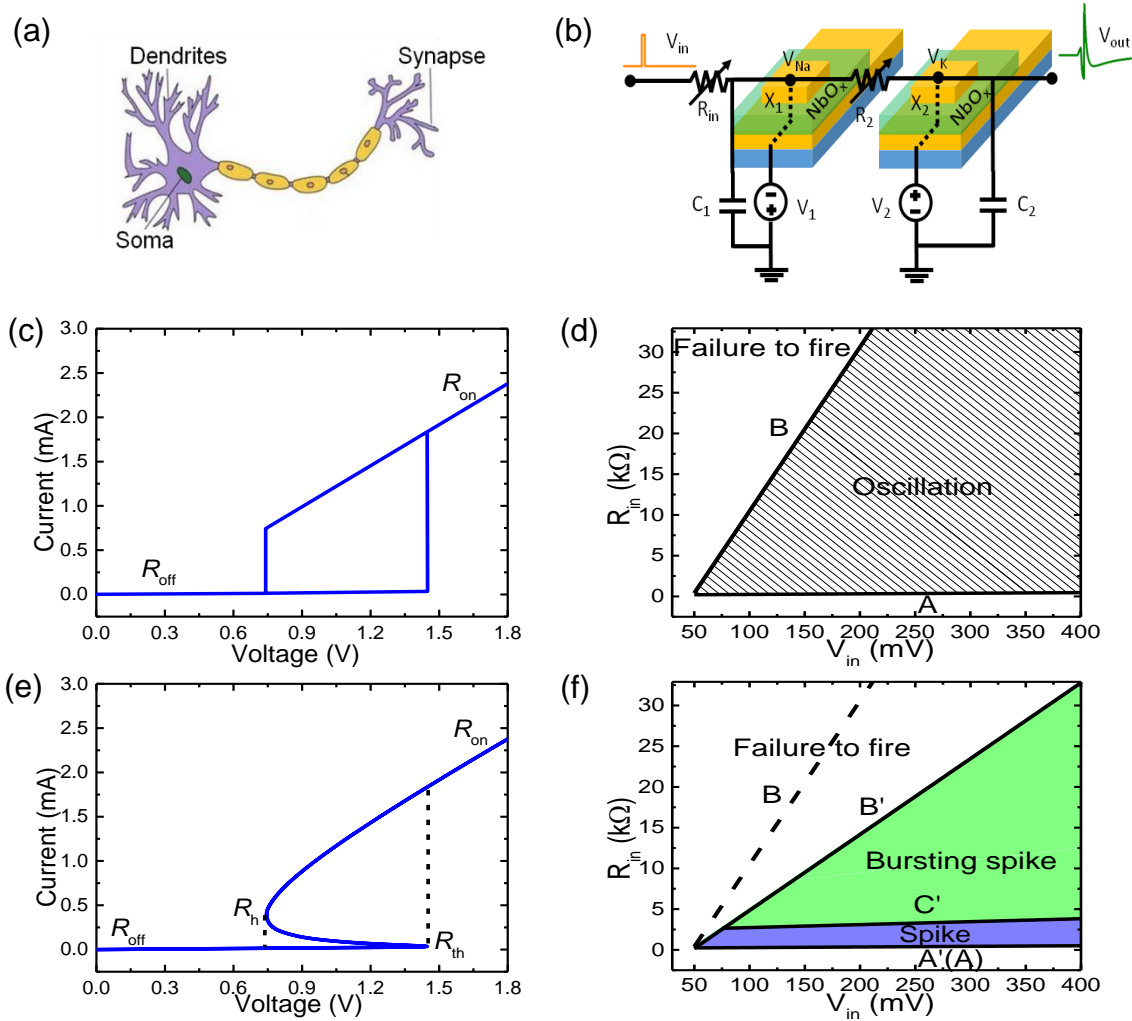


Fig. 1. (a) Schematic structure of a biological neuron. (b) Circuit diagram of memristor neuron composed by two NbO_2 active memristors. (c) I - V curve simulated by the simplest model with fixed values of R_{on} and R_{off} of the memristor and (d) the corresponding operation window diagram calculated by memristor neurons circuit. The two boundaries A and B marked by solid lines divide the window into two areas: failure to fire (white), oscillation (shaded). (e) I - V curve simulated by the IMT model of memristor and (f) the corresponding operation window diagram calculated by memristor neurons circuit. The three boundaries A', B', and C' marked by solid lines divide the window into three areas: failure to fire (white), spike (blue), bursting spike (green). The simulation results of the optimized calculation verified the three boundaries, which is close to the dynamic behavior of the real memristor neurons system. Note that the dashed line is the boundary B marked in (d).

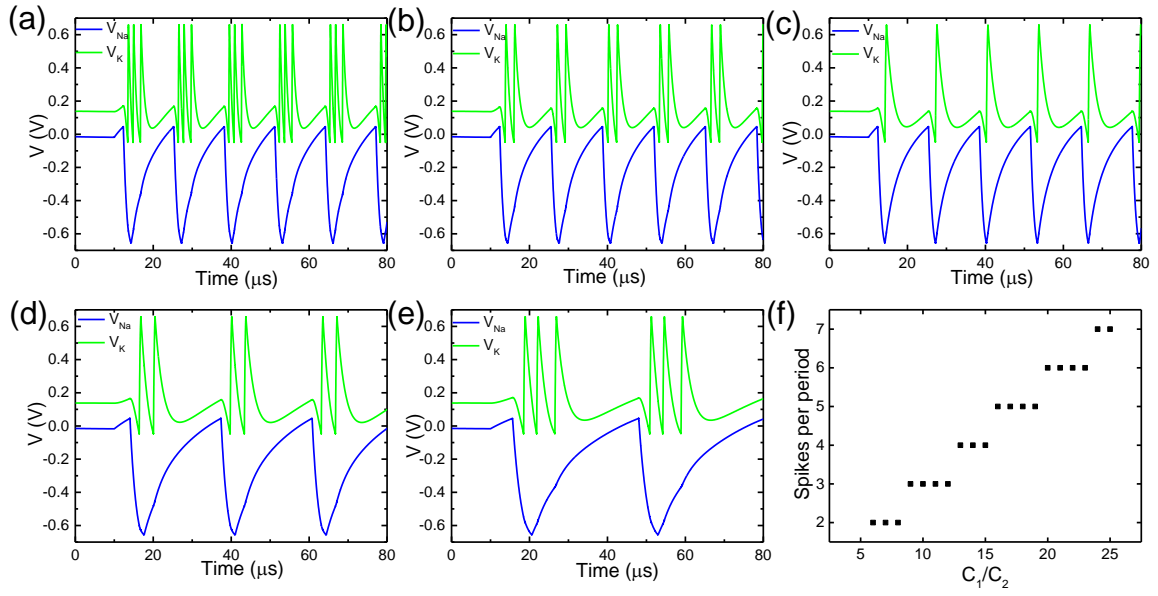


Fig. 2. (a-e) K^+ and Na^+ ion channel voltage waveforms. (a) $C_1=2$ nF, $C_2=0.2$ nF. (b) $C_1=2$ nF, $C_2=0.3$ nF. (c) $C_1=2$ nF, $C_2=0.5$ nF. (d) $C_1=3.5$ nF, $C_2=0.5$ nF. (e) $C_1=5$ nF, $C_2=0.5$ nF. (f) Effect of C_1/C_2 on the number of spikes in each burst period.

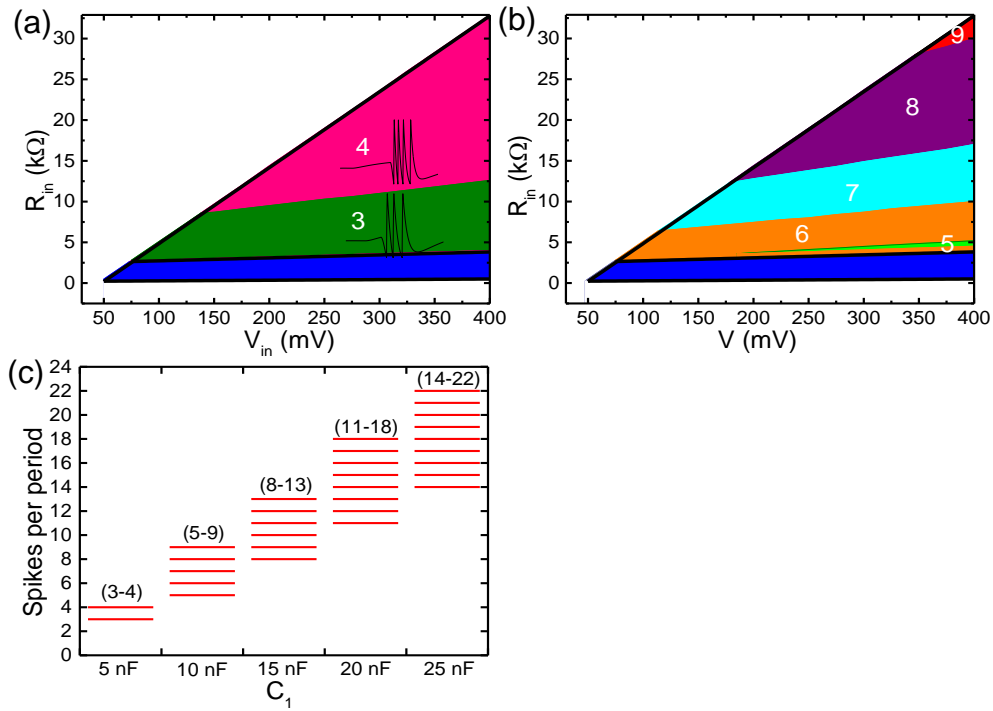


Fig. 3. The simulated operation window of memristor neuron in R_{in} - V_{in} plots, where the used parameters are (a) $C_1=5$ nF, $C_2=0.5$ nF and (b) $C_1=10$ nF, $C_2=0.5$ nF, respectively. The bursting area is divided into some sub-areas according to the number of spikes in each burst period. The insets of (a) show the waveform illustrations of 3 spikes (olive area) and 4 spikes (pink area) per period. (c) The effect of C_1 on the range of the number of spikes per period.

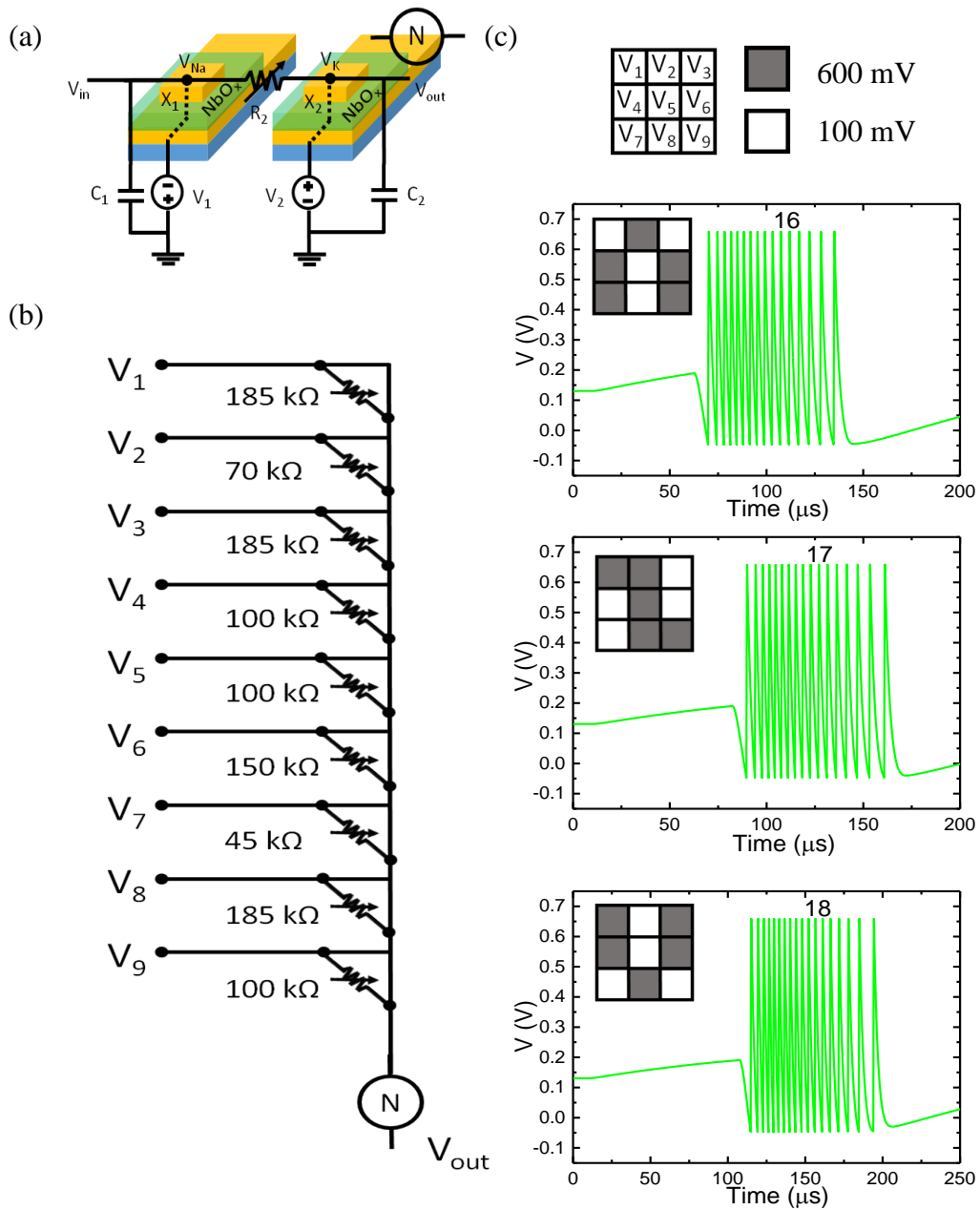


Fig. 4. (a) Memristor neuron symbol and its internal circuit diagram. (c) Schematic of 9x1 array using a memristor neuron. (b) The number of spikes in each burst period of memristor neurons as a response to the 'n', 'z' and 'v' input patterns.

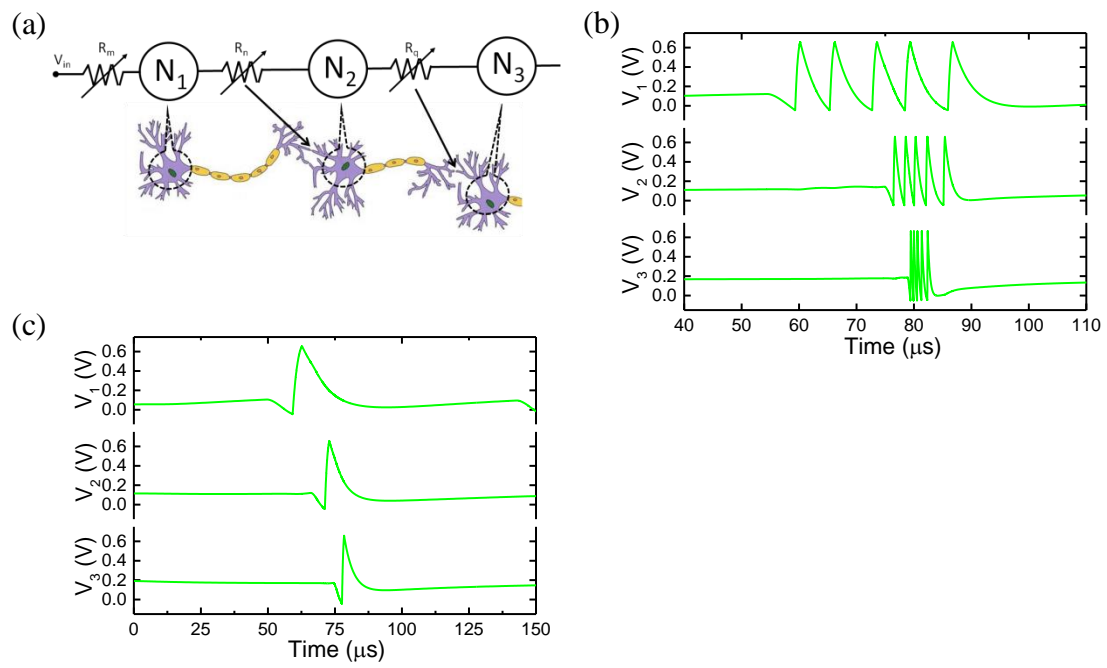


Fig. 5. (a) Schematic diagram of biological neurons and memristor neurons. (b-c) Output signals of neuron N_1 , N_2 and N_3 .

Supplementary material

1) Parameters for circuits and memristor model used in the simulation

Table S1: Parameters used for calculation.

C_1 (nF)	C_2 (nF)	V_1 (V)	V_2 (V)
5	0.5	-1.4	1.4
R_{th} (k Ω)	R_h (k Ω)	R_{off} (k Ω)	R_{on} (k Ω)
41	1.98	49	0.85
V_h (mV)	V_{th} (mV)	R_2 (k Ω)	R_{in} (k Ω)
746	1448	6	0-33

Table S2: Memristor parameters used in the simulation[R1].

Parameter	Model value (SI)	
T_{IMT}	1080 K	Insulator-metal transition temperature
T_{amb}	296 K	Ambient temperature
κ	1.5 W/(m·K)	Thermal conductivity
\hat{c}^p	2.6×10^6 J/(m ³ ·K)	Volumetric heat capacity
ρ_{met}	1×10^{-4} $\Omega \cdot m$	Metallic phase electrical resistivity
ρ_{ins}	7×10^{-3} $\Omega \cdot m$	Insulating phase electrical resistivity
r_{ch}	30 nm	Conduction channel radius
L	20 nm	Conduction channel length
$\Delta \hat{h}^{tr}$	1.6×10^8 J/ m ³	Volumetric enthalpy of transformation

2) Calculation for three main boundaries in R_{in} - V_{in} plots for operational window

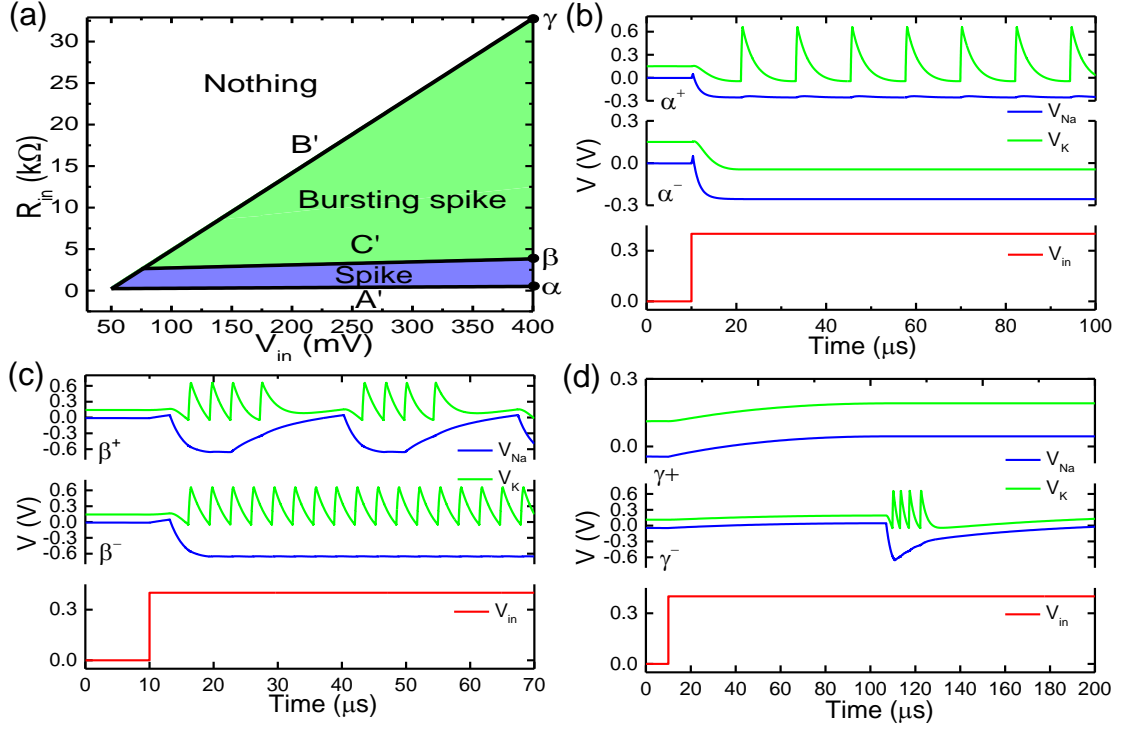


Fig. S1. (a) Simulated and calculated window of R_{in} - V_{in} . The blue area and the green area are simulated window diagrams. The three lines A', B' and C' are theoretically calculated boundary lines. (b-d) Waveforms of V_K and V_{Na} near three points α , β , and γ . Where α^- ($R_{in}=0.504$ k Ω), α^+ ($R_{in}=0.505$ k Ω), β^- ($R_{in}=3.79$ k Ω), β^+ ($R_{in}=3.8$ k Ω), γ^- ($R_{in}=32.9$ k Ω) and γ^+ ($R_{in}=33$ k Ω).

Fig. S1a shows the simulated operational window in R_{in} - V_{in} plots. In order to assist in the study, we select the parameters of the six points α^- ($R_{in}=0.504$ k Ω), α^+ ($R_{in}=0.505$ k Ω), β^- ($R_{in}=3.79$ k Ω), β^+ ($R_{in}=3.8$ k Ω), γ^- ($R_{in}=32.9$ k Ω) and γ^+ ($R_{in}=33$ k Ω) which are located near the upper and lower sides of the three boundary line A', B' and C' of Fig. S1a. The spiking dynamics is described by the membrane potential V_{Na} and V_K as follows[R2]:

$$C_1 \frac{dV_{Na}}{dt} + \frac{V_{Na}-V_1}{R_{X1}} = \frac{V_{in}-V_{Na}}{R_{in}} + \frac{V_K-V_{Na}}{R_2} \quad (S1)$$

and

$$C_2 \frac{dV_K}{dt} + \frac{V_K-V_2}{R_{X2}} = \frac{V_{Na}-V_K}{R_2} \quad (S2)$$

The V_{Na} and V_K waveform of the point α^- and α^+ is as shown in Fig. **S1b**. Before transitioning from α^- to α^+ , the threshold switch X_1 is in a metallic state and the threshold switch X_2 is in a critical state in which the insulating state transitions to a metallic state, $V_2 - V_K = V_{th}$. It can be seen from α in Fig. **S1b** that $\frac{dV_{Na}}{dt} \approx 0$ and $\frac{dV_K}{dt} \approx 0$ after the circuit is stable. Bringing the limit condition back to equations (1) and (2), the equation at the boundary line **A'** is as follows:

$$R_{in} = mV_{in} + m\left(\frac{V_{th}(R_{X2}+R_2)}{R_{X2}} - V_2\right) \quad (S3)$$

$$\text{and} \quad m = \frac{R_{X1}R_{X2}}{R_{X2}(V_2-V_1-V_{th})-V_{th}(R_2+R_{X1})} \quad (S4)$$

for case of $R_{X1} = R_{on}$ and $R_{X2} = R_{th}$.

The V_{Na} and V_K waveform of the point β^- and β^+ is as shown in Fig. **S1c**. When transitioning from β^- to β^+ , bursting activity correspond to an infinite spike train interrupted by short periods of quiescence. The threshold switch X_1 is in a critical state in which the metallic state transitions to an insulating state, the threshold switch X_2 is in a critical state in which the insulating state transitions to a metallic state, $V_2 - V_K = V_{th}$, $V_{Na} - V_1 = V_h$. At the transition point of the graph δ , $\frac{dV_{Na}}{dt} \approx 0$. Bringing the limit condition back to equations (1) and (2), the equation at the boundary line **B'** is as follows:

$$R_{in} = nV_{in} + n(V_h + V_1) \quad (S5)$$

$$\text{and} \quad n = \frac{R_{X1}R_2}{R_2V_h - R_{X1}(V_2 - V_{th} - V_h - V_1)} \quad (S6)$$

for case of $R_{X1} = R_h$.

Fig. **S1d** shows the V_{Na} and V_K waveforms of point γ^- and γ^+ . When transitioning from γ^+ to γ^- , bursting activity correspond to an infinite period of quiescence interrupted by groups of spikes. The threshold switch X_1 is in a critical state in which the insulating state transitions to a metallic state, and the threshold switch X_2 is in an insulating state, $V_{Na} - V_1 = V_{th}$. It can be seen from γ^+ in Fig. **S1d** that $\frac{dV_{Na}}{dt} \approx 0$ and $\frac{dV_K}{dt} \approx 0$ after the circuit is stable. Bringing the limit condition back to equations (1) and (2), the equation at the boundary line **C'** is as follows:

$$R_{in} = qV_{in} + q(V_{th} + V_1) \quad (S7)$$

$$\text{and} \quad q = \frac{R_{X1}(R_2 + R_{X2})}{V_{th}(R_2 + R_{X2}) - R_{X1}(V_2 - V_{th} - V_1)} \quad (S8)$$

for case of $R_{X1} = R_{th}$ and $R_{X2} = R_{off}$, respectively.

3) Other dynamic characteristics of bursting signals

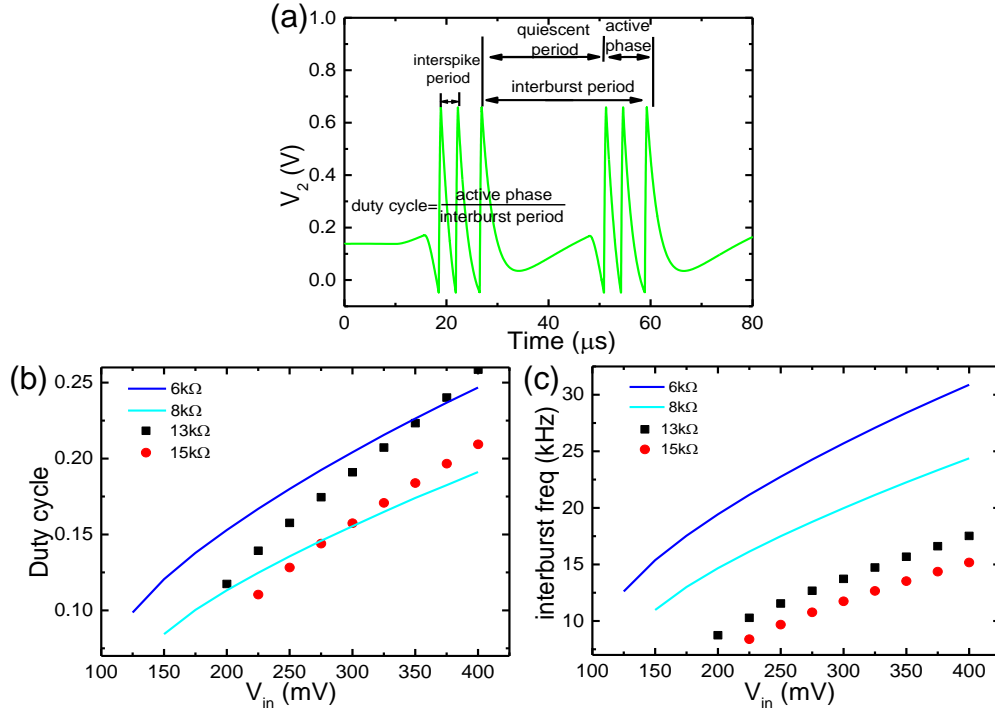


Fig. S2. (a) The bursting spikes of the memristor neuron for defining the new parameter of duty cycle, which is the ratio between the active phase and the interburst period. (b) Duty cycle and (c) the inter-burst frequency as a function of V_{in} , respectively. Both the inter-burst frequency and duty cycle of bursting can be designed as the neuronal information carriers.

Bursting provide two important information: interburst frequency and duty cycle. The interburst period includes two parts as the active phase and quiescent period, as shown in Fig. S2a. The duty cycle is defined as

$$duty\ cycle = \frac{T_{active\ phase}}{T_{interburst\ period}} \quad (1)$$

Using the circuit parameters in Table S1, $R_{in} = 6\text{ k}\Omega$, $8\text{ k}\Omega$, $13\text{ k}\Omega$, and $15\text{ k}\Omega$ are selected in 3 spikes (lines) and 4 spikes (scatters) bursting areas to obtain the

relationship between V_{in} and duty cycle, as shown in Fig. **S2b**. The duty cycle increases with increasing V_{in} in the same spikes area. When the input voltage is fixed, the larger the input resistance, the smaller the duty cycle.

$R_{in} = 6 \text{ k}\Omega$, $8 \text{ k}\Omega$, $13 \text{ k}\Omega$, and $18 \text{ k}\Omega$ are selected in 3 spikes (line) and 4 spikes (point) bursting areas to obtain the relationship between V_{in} and inter-burst frequency, as shown in Fig. **S2c**. The inter-burst frequency increases as the V_{in} increases. The duty cycle and interburst frequency can change as the input changes, which means that information can be encoded into the duty cycle and inter-burst frequency.

References:

- [R1] Pickett M D and Williams R S 2012 Sub-100 fJ and sub-nanosecond thermally driven threshold switching in niobium oxide crosspoint nanodevices *Nanotechnology* **23** 215202
- [R2] Lim H, Kornijcuk V, Seok J Y, Kim S K, Kim I, Hwang C S and Jeong D S 2015 Reliability of neuronal information conveyed by unreliable neuristor-based leaky integrate-and-fire neurons: a model study *Scientific reports* **5** 9776